AD-A053 853 NAVAL OCEAN SYSTEMS CENTER SAN DIEGO CA F/G 9/1
DEVELOPMENT OF A TRIPLE-PRODUCT CONVOLVER USING ZINC OXIDE ON S--ETC(U)
SEP 77 E C JELKS
UNCLASSIFIED NOSC/TR-218 NL

| OF |
AD
A053853

END
DATE
FILMED
6 -78
DDC

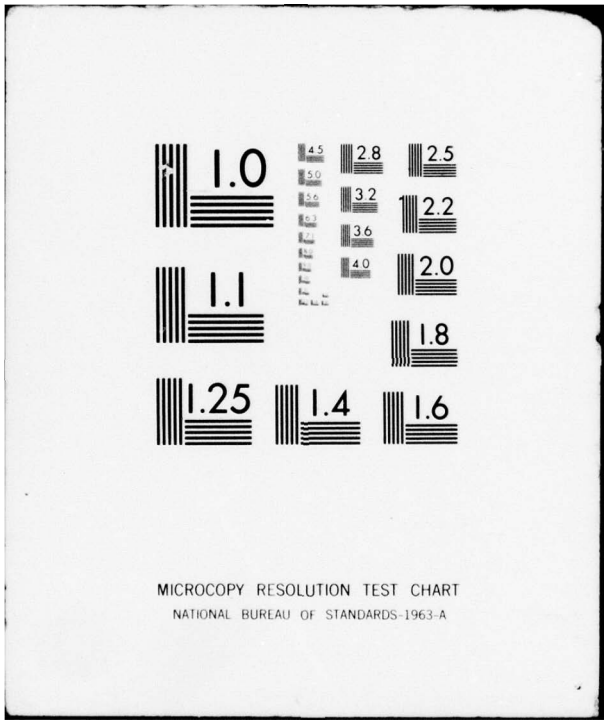
1.0
1.1
1.25
1.4
1.6
1.8
2.0
2.2
2.5
2.8
3.2
3.6
4.0
4.5
5.0
MICROCOPY RESOLUTION TEST CHART
NATIONAL BUREAU OF STANDARDS-1963-A

NOSC TR 218

NOSC

NOSC TR 218

Technical Report 218

DEVELOPMENT OF A TRIPLE-PRODUCT CONVOLVER USING ZINC OXIDE ON SILICON

EC Jelks

30 September 1977

Research and Development Report: October 1976 — September 1977

Prepared For
Technical Director, NOSC

APPROVED FOR PUBLIC RELEASE; DISTRIBUTION UNLIMITED

NAVAL OCEAN SYSTEMS CENTER
SAN DIEGO, CALIFORNIA 92152

NAVAL OCEAN SYSTEMS CENTER, SAN DIEGO, CA 92152

AN ACTIVITY OF THE NAVAL MATERIAL COMMAND

RR GAVAZZI, CAPT, USN
Commander

HL BLOOD
Technical Director

ADMINISTRATIVE INFORMATION

The work in this report was performed under the Center's Independent Research/ Independent Exploratory Development (IR/IED) funds (62766ZF61 ZD18538A01). Work was performed from September 1976 through October 1977 in the Electronic Sciences Branch.

Released by
EB Tunstall, Head
Environmental Acoustics Division

Under authority of
JD Hightower, Head
Environmental Sciences Department

UNCLASSIFIED

SECURITY CLASSIFICATION OF THIS PAGE *(When Data Entered)*

REPORT DOCUMENTATION PAGE

READ INSTRUCTIONS BEFORE COMPLETING FORM

1. REPORT NUMBER: NOSC/TR-218

2. GOVT ACCESSION NO.

3. RECIPIENT'S CATALOG NUMBER

4. TITLE (and Subtitle): DEVELOPMENT OF A TRIPLE-PRODUCT CONVOLVER USING ZINC OXIDE ON SILICON

5. TYPE OF REPORT & PERIOD COVERED: Research and Development Oct 76 - Sept 77

6. PERFORMING ORG. REPORT NUMBER

7. AUTHOR(s): E. C. Pelks

8. CONTRACT OR GRANT NUMBER(s)

9. PERFORMING ORGANIZATION NAME AND ADDRESS
Naval Ocean Systems Center
San Diego, California 92152

10. PROGRAM ELEMENT, PROJECT, TASK AREA & WORK UNIT NUMBERS
NOSC
ZD 18538A01

11. CONTROLLING OFFICE NAME AND ADDRESS
Naval Ocean Systems Center
San Diego, California 92152

12. REPORT DATE: 30 Sept 1977

13. NUMBER OF PAGES: 40

14. MONITORING AGENCY NAME & ADDRESS *(if different from Controlling Office)*

15. SECURITY CLASS. *(of this report)*: UNCLASSIFIED

15a. DECLASSIFICATION/DOWNGRADING SCHEDULE

16. DISTRIBUTION STATEMENT *(of this Report)*

Approved for public release; distribution unlimited.

17. DISTRIBUTION STATEMENT *(of the abstract entered in Block 20, if different from Report)*

18. SUPPLEMENTARY NOTES

19. KEY WORDS *(Continue on reverse side if necessary and identify by block number)*

Zinc Compounds, Silicon, Substrates, Signal Processing

20. ABSTRACT *(Continue on reverse side if necessary and identify by block number)*

Triple-product convolution has been demonstrated with two modulated 80 MHz carrier signals and a third signal consisting of a set of dc voltages. This operation was performed in realtime with two different surface acoustic wave (SAW) devices built on silicon substrates. The transduction of SAWs onto silicon is by means of a thin overlying film of zinc oxide, which is deposited by RF sputtering in a partial oxygen atmosphere. Transducer patterns are defined by "lift-off" photolithography. Good predictions of steady-state device behavior were made using mathematical models, although observed long term memory effects, probably associated with trapping of charge in the ZnO and the Si/SiO_2 interface, are not fully understood.

DD FORM 1 JAN 73 1473 EDITION OF 1 NOV 65 IS OBSOLETE S/N 0102-LF-014-6601

UNCLASSIFIED

SECURITY CLASSIFICATION OF THIS PAGE *(When Data Entered)*

393 159

ABSTRACT

Triple-product convolution has been demonstrated with two modulated 80 MHz carrier signals and a third signal consisting of a set of D.C. voltages. This operation was performed in real-time with two different surface acoustic wave (SAW) devices built on silicon substrates. The transduction of SAWs onto silicon is by means of a thin overlying film of zinc oxide, which is deposited by R.F. sputtering in a partial oxygen atmosphere. Transducer patterns are defined by "lift-off" photolithography. Good predictions of steady-state device behavior were made using mathematical models, although observed long term memory effects, probably associated with trapping of charge in the ZnO and at the Si/SiO_2 interface, are not fully understood.

OBJECTIVES

The primary objective of this study was to characterize and build a surface acoustic wave (SAW) device using thin films of zinc oxide (ZnO) on silicon to demonstrate the triple-product convolution of electrical signals. The secondary objective was to study the transduction of SAWs on silicon, as opposed to standard piezoelectric substrates, with the idea of eventually integrating external circuitry onto SAW devices.

RESULTS

1. A reactive sputtering process, developed in the thin-film laboratory at NOSC, was used successfully in growing highly oriented films of ZnO on glass, gold, titanium, and silicon for SAW transducers.

2. A "lift-off" process for photolithography was developed to produce gold and aluminum patterns on various substrates; patterns were produced with dimensions of less than 5×10^{-6} metre.

3. A general computer program was developed to generate SAW masks using a Gerber plotter for a variety of SAW device geometries.

4. Computer programs were developed to calculate device impedance and mismatch loss as functions of frequency for layered structures, such as $ZnO/SiO_2/Si$.

5. Surface acoustic waves were generated efficiently on glass and silicon substrates, and the measured insertion losses compared favorably with those of computer simulations.

6. Complex optical and electrical memory effects were observed in SAW transducers without a ground plane at the SiO_2/ZnO interface; presumably, they were associated with bulk traps in the ZnO and surface traps on the Si.

7. Triple-product convolution was demonstrated with 4- and 16-tap SAW devices.

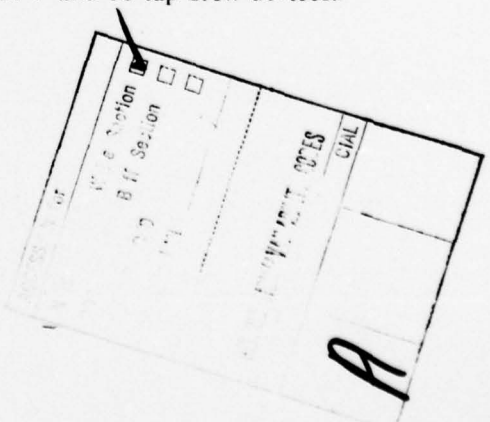

RECOMMENDATIONS

It is recommended that work on the triple-product convolver be continued to make the device practical for use as a Fourier transformer and as a memory convolver for pulse compression. This work should center on eliminating or controlling the optical and electrical memory effects, improving the signal-to-noise ratio, improving bonding and packaging techniques, and developing external circuitry for future integration on the chip.

CONTENTS

INTRODUCTION

The objective of the work described in this report was to build a monolithic delay line device that could form a product from three input signals in real time at various positions along the delay path. A schematic of this new process is shown in figure 1. It can be seen that two of the input signals, $f_1(t)$ and $f_2(t)$, are oppositely propagating waves in the delay medium, while the third input signal, g_i, scales the product of the two propagating waves at discrete positions along the propagating path.

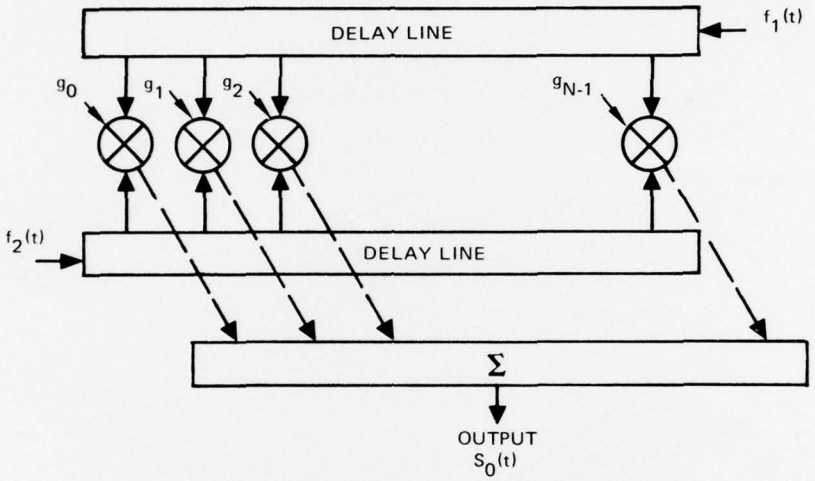

Figure 1. Triple-product convolver.

The importance of such a device lies in the fact that it can be used to perform several useful signal-processing functions, including electrically programmable correlation or convolution and real-time Fourier transforms where the input function is in a parallel format. In the case of the Fourier transform, the two oppositely propagating waves can be modulated with FM signals so that the distributed product along the delay path is a linear function of modulation frequency with distance. This can be visualized by studying the product of two, propagating, linear FM (chirp) waves:

$$\exp\left[j\mu\left(t-\frac{x}{v}\right)^2\right]\cdot\exp\left[-j\mu\left(t+\frac{x}{v}\right)^2\right]=\exp\left[-j\left(\frac{2\mu x}{v}\right)t\right].$$

Thus the frequency of the resultant wave is a linear function of position. If the function to be transformed is now sampled at equal intervals and if each sample is used as the scaling signal at evenly spaced taps along the delay path, then the sum of the output products from all taps is

$$S_0(t)\underset{\sim}{\propto}\sum_i g(x_i)\exp\left[-j\left(\frac{2\mu x_i}{v}\right)t\right].$$

A time-sampled version of this signal is proportional to the discrete Fourier transform (DFT) of $g(x_i)$.

The only known device capable of performing triple-product convolution utilizes surface acoustic waves (SAWs) as the propagating input signals.[1] In the usual SAW devices, a high-frequency electrical signal is applied to a periodic metal pattern deposited on the surface of a piezoelectric crystal (figure 2). If the frequency of the electrical signal and the spacing of the metal pattern are adjusted so that their product equals the natural phase velocity of the crystal, a surface acoustic wave will be generated that will propagate a long distance on the crystal with very little loss of amplitude. Since the energy in the wave is confined to a region at the crystal's surface, the wave may be tapped at any point in its path with another periodic metal pattern.

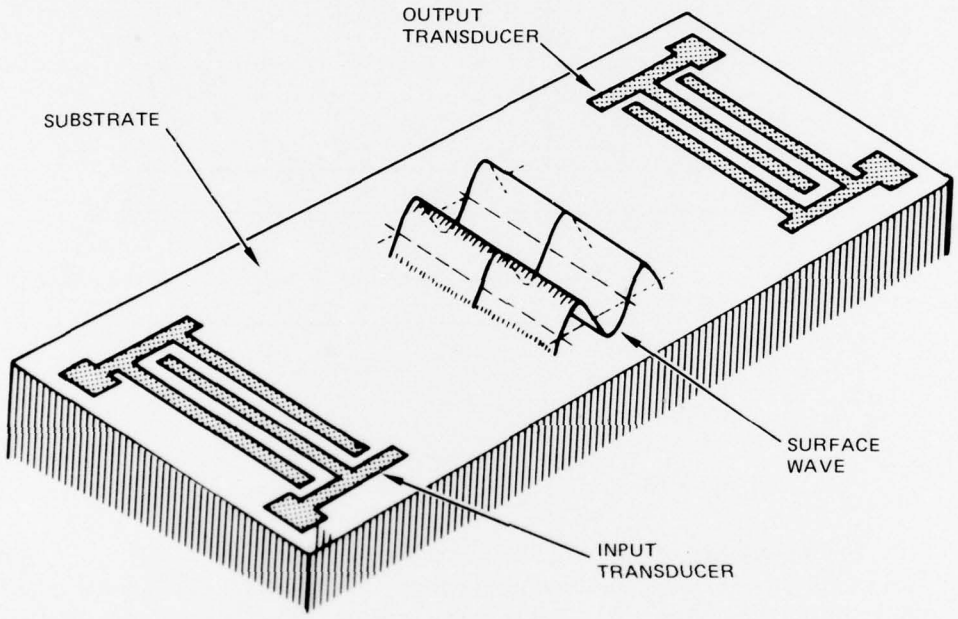

Figure 2. A simple surface acoustic wave device.

In the case of the triple-product convolver, discrete Schottky diodes have been used as nonlinear tap elements[1]. The two primary drawbacks to this approach are the necessity of using hybrid techniques and the strong nonlinearity of the output Fourier coefficients as a function of the tap-scaling input signals. To address these problems, two monolithic devices have been conceived, both using silicon as the delay medium. The first uses MOSFETs (metal-oxide semiconductor field-effect transistors) as the nonlinear tap elements and the piezoresistance of silicon as the method of achieving transduction of the SAWs to electrical signals. Since silicon is not a piezoelectric material, the launching of the SAWs is through an intermediate piezoelectric film deposited on the silicon substrate. The second device, also using piezoelectric films to launch SAWs, uses MOS capacitors as the nonlinear tap elements. It was decided to pursue the second device, as it could be fabricated almost entirely at NOSC's thin-film laboratory and because the Fourier output was expected to have a greater

1. Reeder, T.M., "Fourier Transformation of Television Signals by Nonlinear Delay Line Techniques," United Aircraft Research Laboratories Technical Report N921957-F, March 1975.

linear dynamic range with applied input than would be possible with the first approach (appendix A).

To clarify the ideas behind the nonlinearity of a MOS capacitor tap, figure 3 is instructive. When a negative bias is applied to the metal tap of the metal/oxide/n-type semiconductor sandwich, the free electrons contributed by the donor impurities are driven from

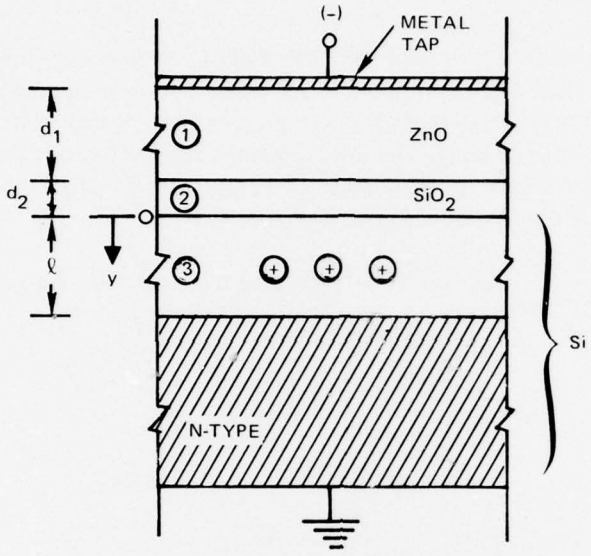

Figure 3. MOS tap structure.

the region of the semiconductor directly under the metal tap, leaving this region depleted of free carriers. This depleted region consists of a uniform distribution of uncovered immobile donor impurities, each having a positive charge. The solution to Poisson's equation in the depleted region is (appendix B)

$$\phi_3(y) = -\frac{qN}{2\epsilon_3}y^2 + \frac{qN\ell}{\epsilon_3}y - \frac{qN\ell^2}{2\epsilon_3}$$

and

$$E_3(y) = -\frac{d\phi_3(y)}{dy} = -\frac{qN}{\epsilon_3}y + \frac{qN\ell}{\epsilon_3} \quad ,$$

where ϕ_3 is the electric potential in the silicon, q is the electronic charge, N is the donor charge density, ϵ_3 is the electrical permittivity of the silicon, and ℓ is the depletion width. The potential at the surface of the silicon substrate is then

$$\phi_3(0) = -\frac{qN\ell^2}{2\epsilon_3} = \frac{\epsilon_3}{2qN}E_3^2(0)$$

If the static electric field is perturbed by a time-varying electric field $E_{31}(0)$ carried by a propagating piezoelectric surface wave, the resulting small signal potential $\phi_{31}(0)$ is approximately

$$\phi_{31}(0) \approx \frac{\epsilon_3}{2\,q\,N}\,[2\,E_3(0)\,E_{31}(0) + E_{31}^2(0)] \quad .$$

Therefore, the silicon surface potential will have a major component proportional to the square of the electric field carried by the surface wave. The fact that this second harmonic component can be linearly scaled with bias voltage does not appear in this simplified analysis, since the "nonabrupt" nature of the depleted region is responsible for the effect. A plot of the theoretical variation of the second harmonic component as a function of bias voltage, based on a more detailed analysis, is shown in figure 4.[2]

2. Kino, G.S., and Gautire, H., "Convolution and parametric interaction with semiconductors," *J. Appl. Phys.*, vol. 44, no. 12, 5219 (1973).

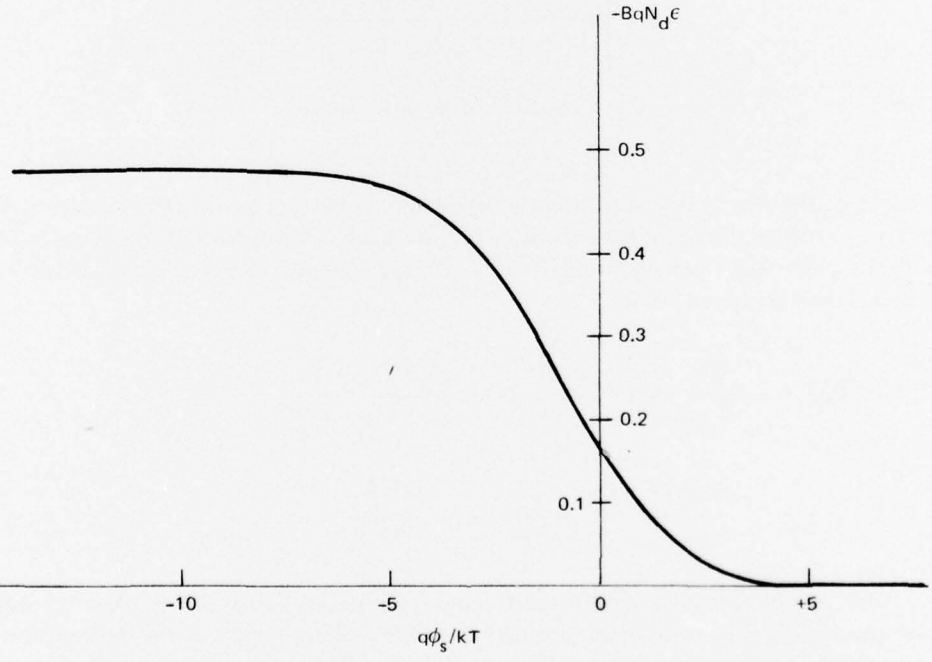

Figure 4. Nonlinear coupling coefficient as a function of silicon surface potential for n-type silicon.

PROCESS DEVELOPMENT

ZINC-OXIDE FILMS

The first step in developing the trip-product convolver was to learn how to grow thin piezoelectrically active films for coupling acoustic energy into the silicon substrate. Zinc oxide (ZnO) was chosen as the piezoelectric film because of its large piezoelectric coupling factor and because such films already had been grown successfully by a few laboratories for SAW applications.[3] These films are usually RF sputtered. Since most RF sputtering systems are unique and since RF sputtering is largely an empirical technique, an experimental program was embarked upon to develop a repeatable ZnO process for the existing system at NOSC.

The major modifications to the system were the installation of a high-purity ZnO target, the construction and installation of a temperature controlled substrate holder, the installation of a laser film thickness monitor, and the addition of an 80-percent argon/20-percent oxygen mixture for the sputtering atmosphere. A schematic of the completed system is in figure 5. The substrate holder was designed to be vacuum tight to prevent outgassing of the heater into the vacuum chamber. The thickness monitor was based on the idea of continuously observing the reflection of a laser from the transparent ZnO film and noting where the interference nulls occurred as a function of time. If it is assumed that the film deposition is linear with time, a trial film deposition run allows calibration of the laser output record in angstroms per interference fringe.

---

3. Hickernell, F. S., and Brewer, J. W., "Surface-elastic-wave properties of dc-triode-sputtered zinc oxide films," *Appl. Phys. Lett.*, vol. 21, no. 8, 389 (1972).

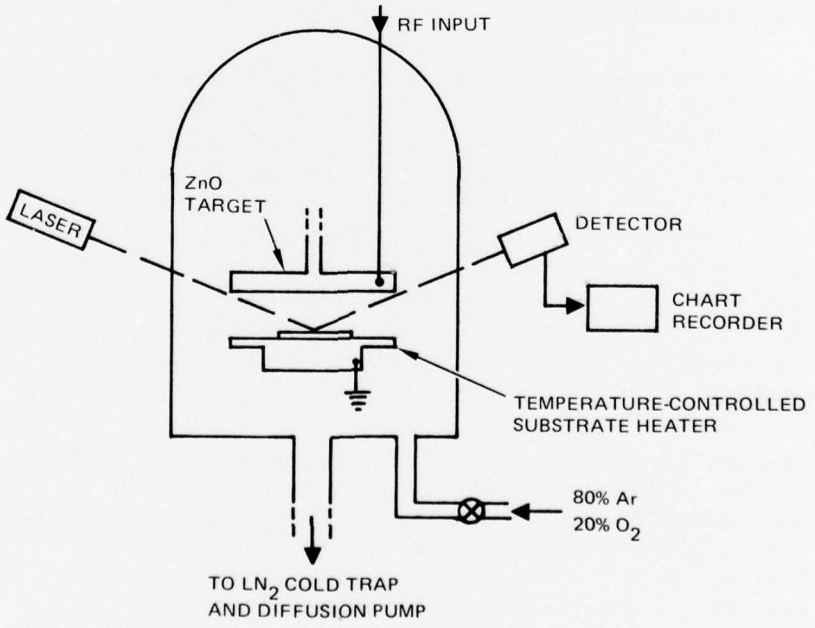

Figure 5. Schematic of ZnO sputtering apparatus.

To launch surface acoustic waves efficiently onto a layered structure consisting of a piezoelectric film on a nonpiezoelectric substrate, it is necessary for the major piezoelectric axis of the film to be in a direction normal to the substrate. Since ZnO films have isotropic piezoelectric properties in a plane normal to the main piezoelectric axis, or Z axis, only polycrystalline films need be grown as long as the Z axes of the crystallites are vertical. Previous experiments by workers in the field have shown that ZnO films tend to orient with the Z axis in the direction of the incident atoms, if the deposition rate is low enough and the substrate hot enough to allow sufficient molecular mobility on the substrate after condensation. At temperatures in excess of 300°C and deposition rates around 200 angstroms per hour, the films can become epitaxial.[4]

The first film deposition runs were made using glass microscope slides as substrates and adjusting the system parameters approximately to those used by Khuri-Yakub.[5] Checks on film orientation were made initially with the use of the X-ray diffraction system at NOSC; the Z axis orientation was judged according to the relative magnitudes of the reflections from the three principal planes. It was found that for substrate temperatures in excess of approximately 120°C, X-ray reflections from the (101) and (100) planes were indiscernable in the noise with a deposition rate of 150 angstroms per minute. Figure 6 shows X-ray data from a well oriented film of ZnO on glass. The reflections from the (101) plane at 36.5 degrees and the (100) plane at 31.5 degrees are absent. Similar experiments were carried out on gold, titanium, aluminum, and SiO_2. Adherence to the gold was a problem because of the inability of gold to form good chemical bonds with the ZnO; however, a 200-angstrom layer of titanium between the gold substrate and the ZnO film cured the problem with the additional advantage of less ZnO film surface roughness. It was found that well oriented films of ZnO could be grown on all the substrates, with a deposition rate of 150 angstroms per minute and a substrate temperature of 200°C.

PHOTOLITHOGRAPHY

Standard integrated-circuit photolithographic techniques normally are not suitable for fabricating devices with ZnO on silicon, since the etching required to delineate metal patterns in most cases affects the ZnO. Consequently, a photolithographic technique without etching had to be developed in the NOSC laboratory. The process chosen was patterned after one called "lift-off" which is used by some surface-wave and integrated-optics laboratories.[6] The basic process sequency is pictured in figure 7, and consists of (1) spinning a layer of positive photoresist onto the substrate, (2) exposing the photoresist with ultraviolet light through a prepared photographic mask, (3) developing, or removing, the regions exposed to the light, (4) depositing a thin layer of metal over the developed photoresist pattern, and (5) "lifting-off" the metal lying directly on the photoresist regions by removing the photoresist with a solvent.

---

4. Rozgonyi, G. A., and Polito, W. J., "Epitaxial thin films of ZnO on CdS and Sapphire", *J. Vac. Sci. Tech.*, vol. 6, no. 1, 115 (1969).
5. Khuri-Yakub, B. T., Kino, G. S., and Galle, P., "Studies of the optimum conditions for growth of rf-sputtered ZnO films", *J. Appl. Phys.*, vol. 46, no. 8, 3266 (1975).
6. Smith, H. I., Bachner, F. J., and Etremow, N., "A High-Yield Photolithographic Technique for Surface Wave Devices", J. Electrochem. Soc., vol. 118, no. 5, 821 (1971).

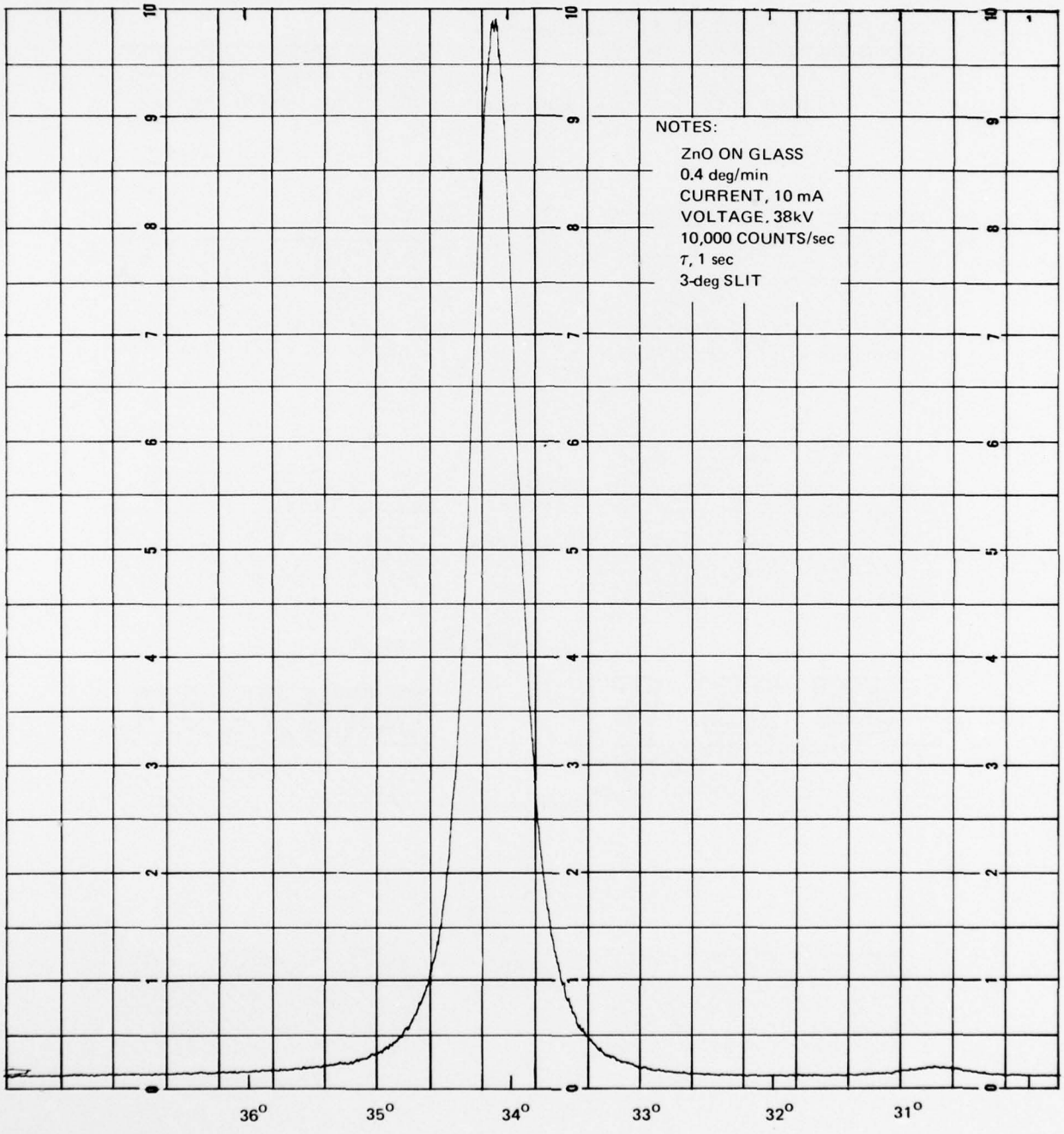

Figure 6. X-ray diffraction from ZnO on glass with substrate temperature controlled at 150°C.

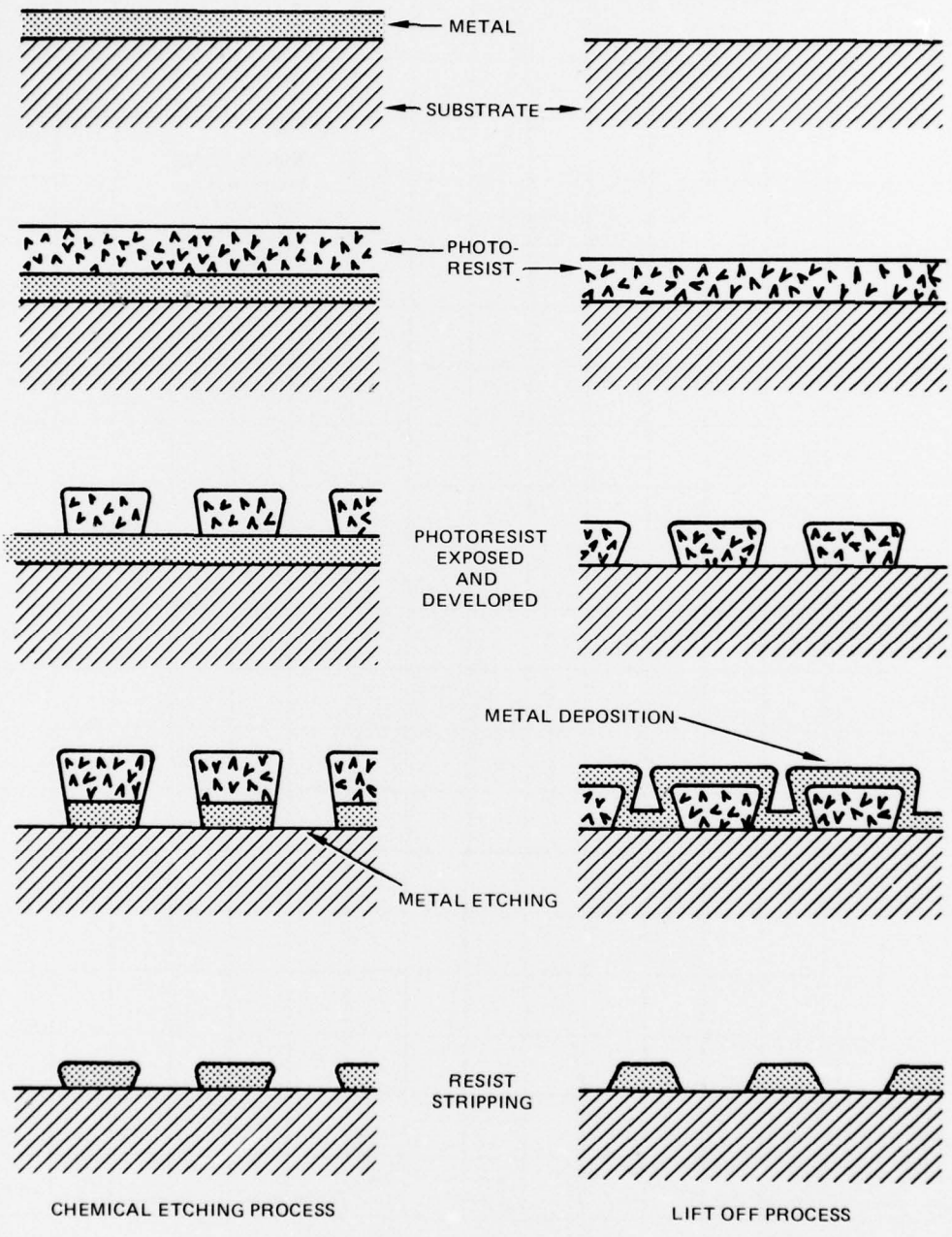

Figure 7. Schematic representation of photolithographic processes.

Success of this technique depends basically on two factors: vertical or undercut photoresist edges after developing and good adhesion of the metal film to the areas of the substrate where the photresist has been removed. A large number of trials were run on glass and ZnO using gold, titanium, and aluminum metallization to establish the best parameters for use with the NOSC laboratory system and the best chemical procedure. The key elements to success with "lift-off" photolithography were found to be (1) a thorough cleaning of the substrates in inorganic solvents when possible and boiling in a detergent solution followed by boiling in deionized water, (2) intimate contact between substrate and mask during exposure, achieved by using vacuum pulldown on the mask and evidenced by visible optical interference fringes at the interface, (3) exposure times in excess of 200 seconds to enhance undercutting, (4) the use of a 300-angstrom titanium film between the substrate and metallization to assure good adhesion, and (5) pressures less than 5×10^{-8} torr in the vacuum chamber before metal deposition to thoroughly out-gas regions of the substrate where photoresist was removed.

Figure 8 shows a properly developed photoresist pattern that is viewed under an electron microscope. The bright lines are indicative of charge buildup at a sharp edge. Figure 9 shows a final metallization pattern that was exposed for too short a time and did not have a titanium adhesion film. Some areas of the metal film did not stick in the desired areas and tearing of the metal along the pattern's boundaries occurred. Figure 10 shows a correctly processed pattern, where the edges are clean and adhesion is good. Good results were obtained to better than 5×10^{-6} metre resolution on all substrates and metals tried, using the procedure listed in appendix C.

MASK GENERATION

To achieve adequate piezoelectric coupling to thin ZnO films, carrier frequencies in excess of 60 megahertz are required for the ZnO-on-silicon devices, which in turn requires high-resolution contact masks for device fabrication. The very small pattern dimensions rule out hand-prepared rubylith masters. Consequently, computer-generated masks had to be developed using the Gerber plotting facilities at NOSC. A general computer program was written to calculate automatically the mask coordinates of a variety of different kinds of SAW device geometries by entering the appropriate parameters into the program. The punched-card output from this program is used as input to the Gerber plotter, which photographically reproduces SAW device geometry onto a large sheet of film that serves as a master mask. This mask is photographically reduced by a factor of ten onto a high resolution photographic plate in the surface wave laboratory. The photoresist film in the substrate is directly exposed through the light and dark pattern on the plate as explained in the previous section.

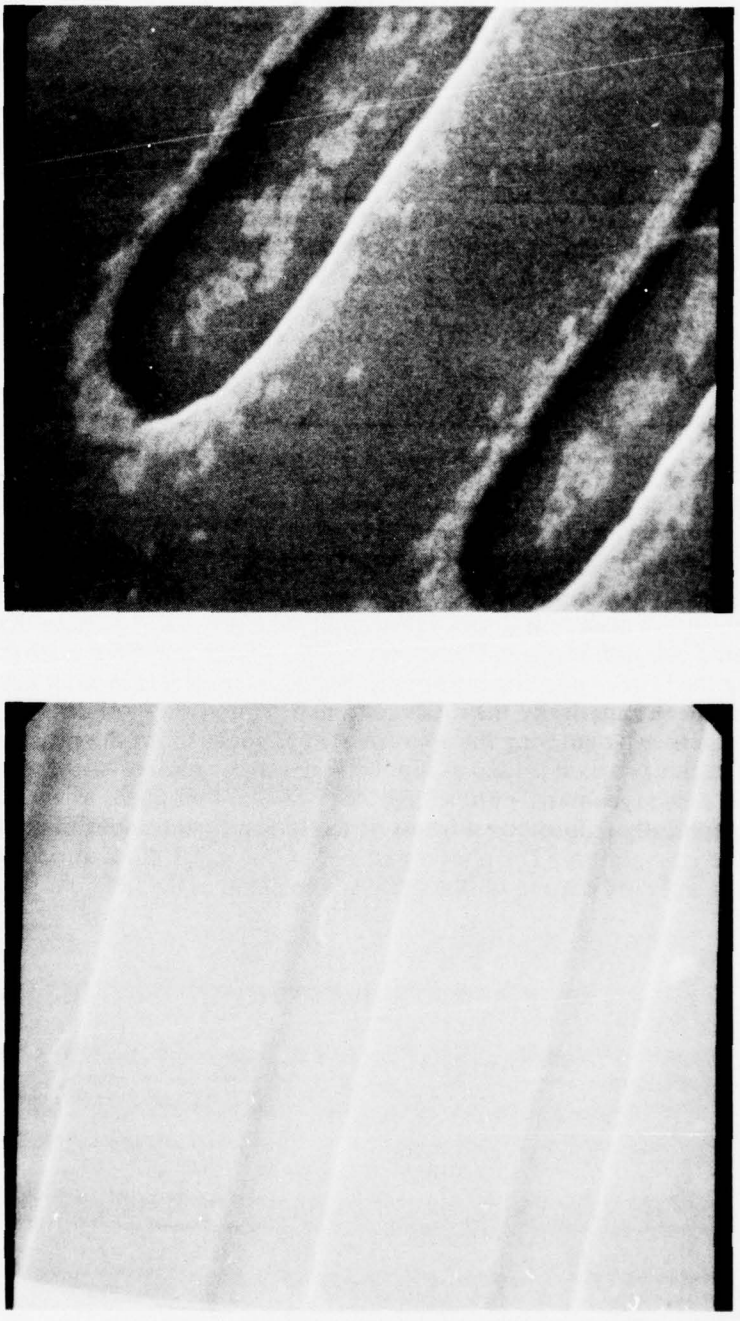

Figure 8. Photoresist patterns on glass viewed under an electron microscope.

Figure 9. Aluminum pattern on glass produced when substrate-mask contact was poor, exposure time was too short (110 seconds), and no titanium layer was used.

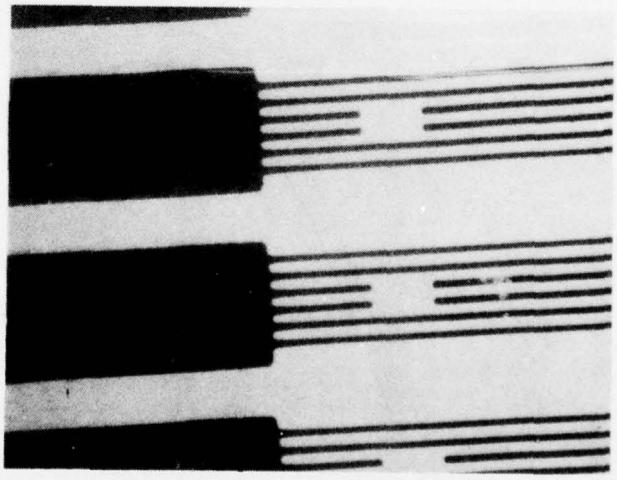

Figure 10. Aluminum pattern on glass produced with good substrate-mask contact, long exposure time (220 seconds), and 300 angstroms of titanium for adhesion.

PROPAGATION OF SAWs ON NONPIEZOELECTRIC SUBSTRATES

OUTLINE OF BASIC THEORY

The equivalent circuit used for the SAW transducer is shown in figure 11. Here, the acoustic impedance of the SAW transducer is broken into real and imaginary parts: R_a and X_a. The radiation resistance R_a accounts for all the power from the generator that is coupled into the propagated surface wave. The other circuit elements are C_T, the capacitance of the

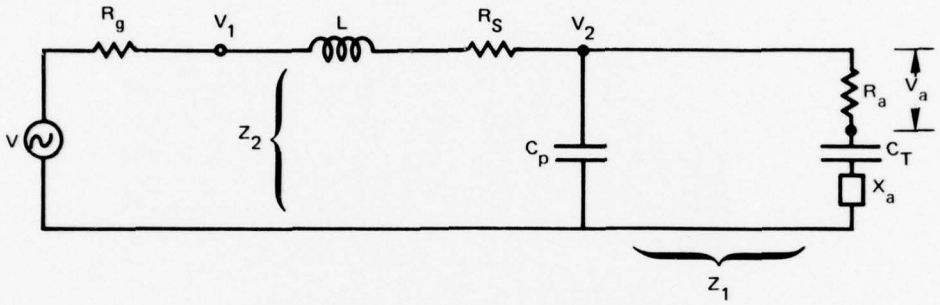

Figure 11. Equivalent circuit for SAW transducer.

metal interdigital transducer; C_p, the stray capacitance from connectors and bonding pads; R_S, the series lead resistance; L, the series tuning inductor; and R_G, the 50-ohm generator resistance. Kino calculated R_a, X_a, and C_T for the four layered geometries shown in figure 12 by using a variational technique.[7] The general form of the acoustic impedance

7. Kino, G. S. and Wagers, R. S., "Theory of interdigital couplers on nonpiezoelectric substrates", *J. Appl. Phys.*, vol. 44, no. 4, 1480 (1973).

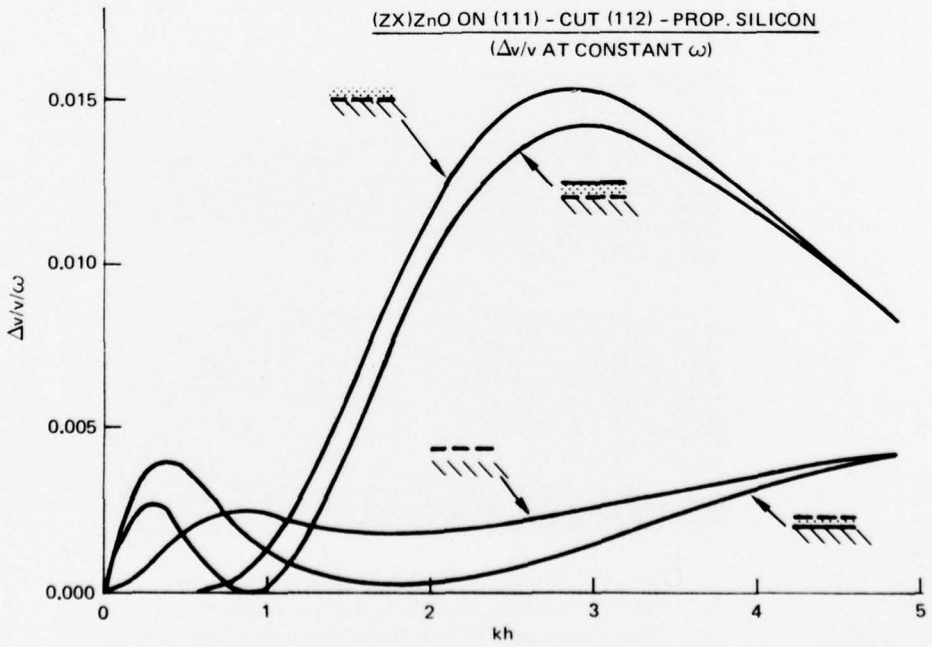

Figure 12. Δv/v versus kh at constant frequency for the ZnO-Si structure with the geometries shown above (see reference 7).

for a layered structure is the same as for a semi-infinite substrate. However, ω (radial frequency) becomes k (wave number) for the layered case because of dispersion:

$$R_a = \hat{R}_a \left(\frac{\sin x}{x}\right)^2$$

and

$$X_a = \hat{R}_a \left(\frac{\sin 2x - 2x}{2x^2}\right) ,$$

where

$$x = \frac{\pi N (k - k_1)}{k_1} , k_1 = \frac{2\pi}{\ell} , N = \text{number of finger pairs.}$$

The expressions for $\hat{R}_a$ and C_T are complicated functions of geometry and material parameters and will not be listed here; however, it is important to note that

$$\hat{R}_a = \underset{\sim}{\alpha} \frac{K^2}{\omega_0 W} ,$$

where K^2 is the piezoelectric coupling constant, ω_0 is the center frequency of the transducer, and W is the transducer aperture width. Thus, in principal, the radiation resistance at the center frequency of a transducer can always be adjusted to 50 ohms for any given coupling constant by adjusting the aperture. However, practical considerations such as diffraction and photolithographic limitations often make this impossible.

To calculate the total frequency-dependent insertion loss of the layered transducer, a computer program was written to solve the circuit in figure 11 (given R_a, X_a, and C_T calculated by a subprogram). This program served as the basis for all surface-wave device designs in developing the triple-product convolver. The procedure developed is as follows. Given a center frequency ω_0, the coupling constant K^2 can be approximated by knowing the ZnO film thickness. This is done by using tabulations as illustrated in figure 12. It can also be done by calculating the perturbations in SAW propagation velocity, caused by the insertion of metal planes in place of the transducer, with procedures such as used by Fahmy.[8] The optimum number of finger pairs is then approximately given by

$$N = \sqrt{\frac{\pi}{4 K^2}} .$$

In this case, optimum means maximum possible bandwidth under the condition of matching the transducer to the source with a series inductor. Using Kino's formulas, the transducer aperture width that gives 50 ohms radiation resistance can be found, as well as C_T. Use of the general equivalent circuit model described in figure 11 allows the calculation of the tuned and untuned insertion losses of the transducer as a function of frequency.

8. Fahmy, A. H., and Adler, E. L., "Multilayer acoustic-surface-wave program," *Proc. IEE*, vol., 122, no. 5, 470 (1975).

An important consideration in designing ZnO-on-silicon devices became apparent as a result of using this program: when high-frequency transducers are used, stray connector and bonding-pad capacitance can significantly decrease the effective radiation resistance seen by the generator because of the small transducer capacitance. A useful approximate way of viewing this was pointed out by Dr. Eric Adler of McGill University (a temporary employee at NOSC during the summer of 1977. For the case where

$$\frac{1}{\omega_0 R_a C_T} >> 1 ,$$

the effective radiation resistance is given approximately by

$$\hat{R}_a \approx R_a \left(\frac{C_T}{C_p + C_T} \right)^2 .$$

As a consequence, it is often impossible to design R_a for 50 ohms because decreasing the aperture not only increases R_a but also decreases C_T (see appendix D). It is sometimes possible to remedy this problem by increasing the number of finger pairs to increase C_T at the expense of reducing the bandwidth of the transducer.

EXPERIMENTAL RESULTS

The first delay lines fabricated with ZnO films consisted of a substrate, ZnO-film, interdigital-transducer geometry to avoid the extra processing step of a film interface ground plane and to eliminate failures from pinholes in the ZnO films. These devices were used to verify the models and estimate the quality of the ZnO films. The first successful launching of a SAW on a nonpiezoelectric substrate was accomplished using a glass microscope slide as a substrate, a 2×10^{-6} metre thick ZnO film, and an aluminum interdigital transducer of 140-megahertz frequency. Figure 13 shows the first observed SAW on glass, which had a one-way midband, untuned mismatch loss of 28 decibels. The calculated insertion loss is shown in figure 14.

Reasonable untuned insertion losses were also observed using (111) silicon with an overlying 2000-angstrom, thermal-oxide layer as a substrate. However, when devices were built on silicon/SiO_2 to observe nonlinearities, several difficulties arose. First, it became clear that series inductor tuning did not give the expected improvement in insertion loss. Also, the different potentials at the bottom of the substrate significantly affected the insertion loss. In addition, DC bias applied to the transducers and optical illumination drastically affected the insertion loss, with the added complication of long-term memory effects.

Careful observation revealed that the influence of the bulk silicon on the transducer equivalent circuit was completely responsible for all the above effects. As a first approximation, the silicon bulk resistance can be entered into the equivalent circuit model by adding a series resistor to R_a. This series resistance does not change the untuned insertion loss significantly, since the large impedance of C_T causes an almost constant current in the circuit. Consequently, the untuned insertion losses measured on the first devices agreed with what was expected. However, when C_T was tuned out, the measured insertion losses

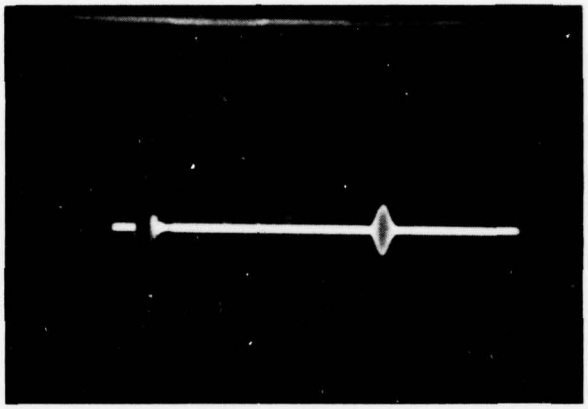

Figure 13. First observed SAW on glass using ZnO film transducers (0.5 microsecond-per-division horizontal scale).

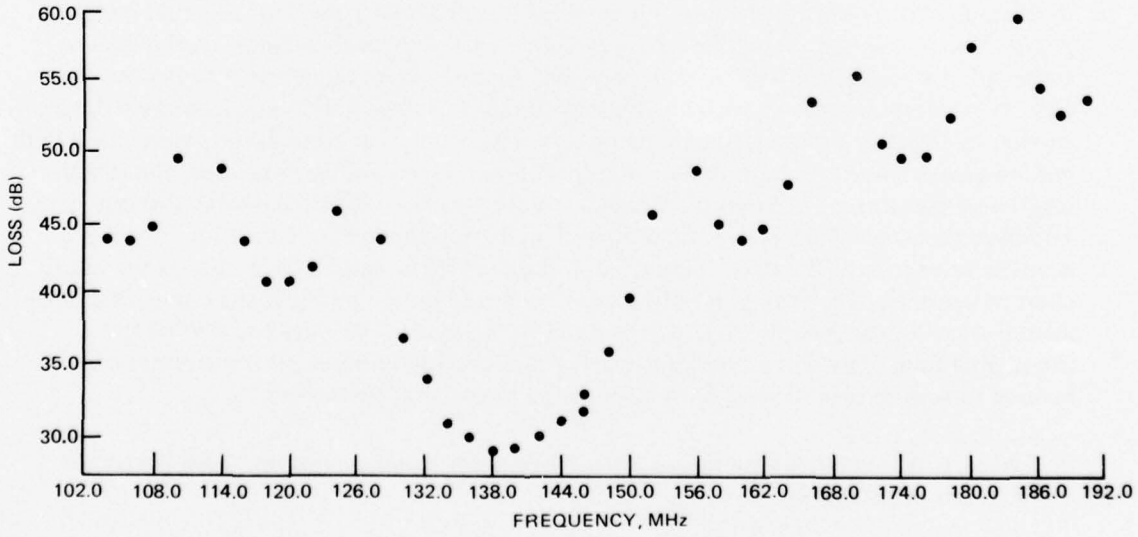

Figure 14. Calculated, one-way, untuned insertion loss for a ZnO on glass transducer (measured midband loss = 28 dB).

were much higher than expected because of the power dissipated in the bulk term (see appendix E). This was confirmed experimentally by immersing the device in liquid nitrogen to decrease the free carrier density in the bulk. The Smith chart data in figure 15 shows the decrease in the transducer series resistance as a result of cooling.

The silicon bulk resistance also enters into the equivalent circuit in a more complicated way as a distributed resistance associated with the bonding pads. This is the primary reason that the insertion loss is affected by the boundary conditions at the bottom of the substrate, since the presence of a ground directly under the bonding pads causes power to be shunted from the transducer to the bulk resistance between the bonding pads and ground. This can be seen in figures 16 and 17. Figure 16 shows Smith chart data on an 80-megahertz transducer with the bottom of the silicon ungrounded, while figure 17 is the same transducer with a grounded region directly under the fingers.

Memory effects apparently arise from the complex interaction of two phenomena: injection of electrons (for n-type silicon) into bulk traps in the ZnO [9] and the filling of traps at the silicon/silicon dioxide interface. One observed memory effect was a bias-dependent retention of insertion loss level, triggered by a light pulse incident on the transducer region. A decrease in insertion loss presumably comes from depleting the free carriers at the silicon surface with the trapped charge, thereby decreasing the attendant electrical dissipation of the surface wave. The long-term trapping of charge generated by optical illumination can be seen in figures 18 and 19. Figure 18 is the capacitance as a function of DC bias of an 80-megahertz interdigital transducer on silicon both in room light and in the dark. Figure 19 shows the decay of charge back to equilibrium after the removal of a large inverting negative voltage from a similar transducer. Although the bias variable storage effects in the ZnO-on-silicon devices appear promising as new signal processing tools, they are detrimental to the operation of a triple-product convolver. Consequently, a detailed study of these effects was not pursued.

It became clear that to achieve the low insertion loss levels necessary for a useful triple-product convolver, a ground shield under the transducer between the ZnO and SiO_2 to shield out the effects of the bulk silicon would be needed (figure 20). The first interface ground shields used on the silicon devices were deposited through stainless steel masks to cover only the transducer region. This was done to avoid extra capacitance to the bonding pads. It was found, however, that the bulk resistance from the bonding pads was still large enough to affect significantly the insertion loss. Therefore, two more devices were made with ground planes covering a large region around the transducer, and in these cases the tuned insertion losses dropped to expected values (36 decibels for a 0.34-millimetre aperture with 10 finger pairs and 24 decibels for a 0.60-millimetre aperture with 15 finger pairs). The acoustic resonance of the 0.6-millimetre transducer at 80 megahertz is shown on the Smith chart in figure 21. The radiation resistance is evidenced by the hump in the curve. One detrimental effect of the ground plane was to decrease R_a by four because one-half of the interdigital fingers were at ground potential. A balanced-to-unbalanced transformer can be used to restore operation of both sides of the interdigital transducer.

---

9. Coldren, L. A., "Effect of bias field in a zinc-oxide-on-silicon acoustic convolver," *Appl. Phys. Lett.*, vol. 25, no. 9, 473 (1974).

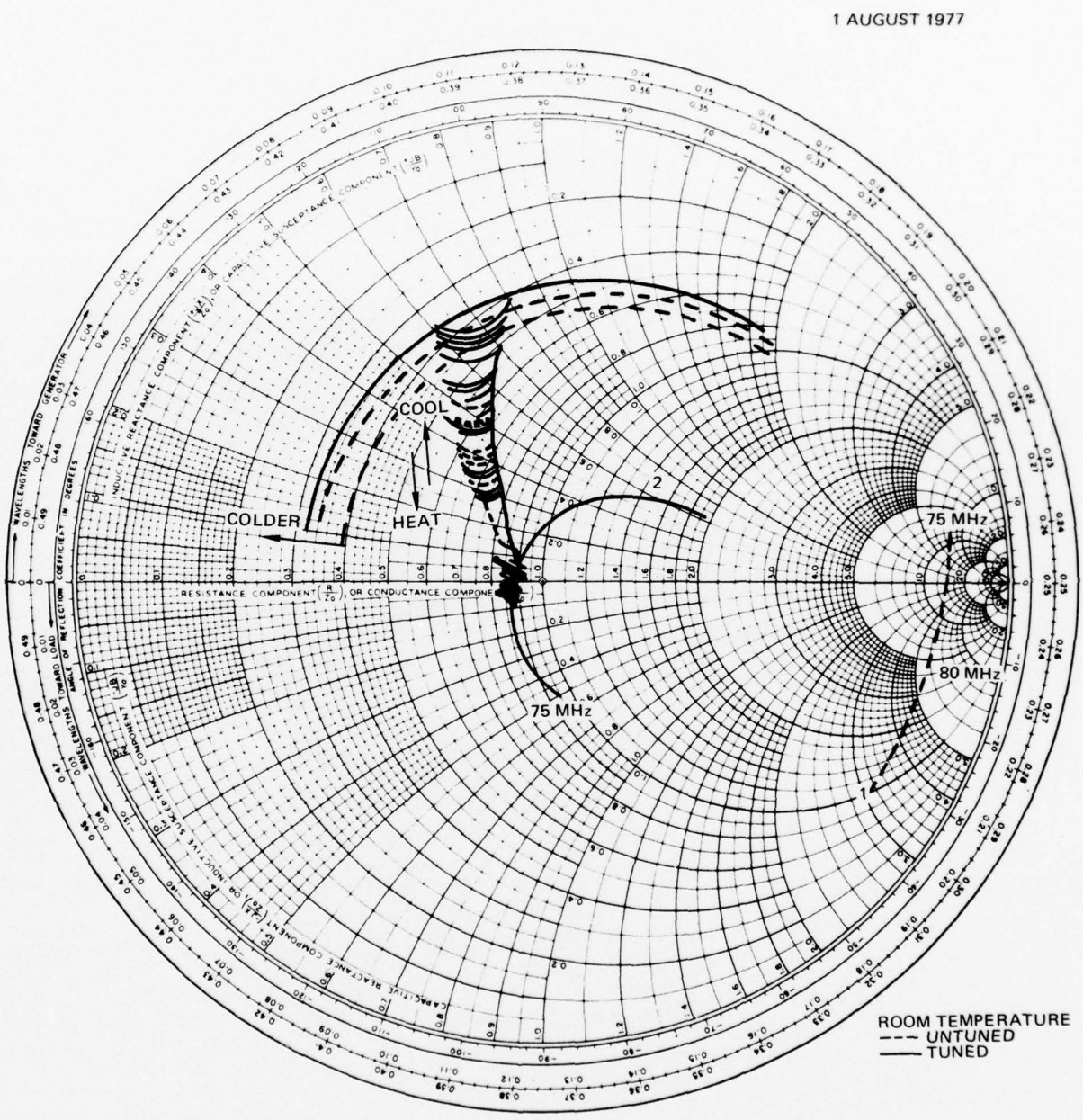

Figure 15. Variation of transducer impedance when cooled to 77° K.

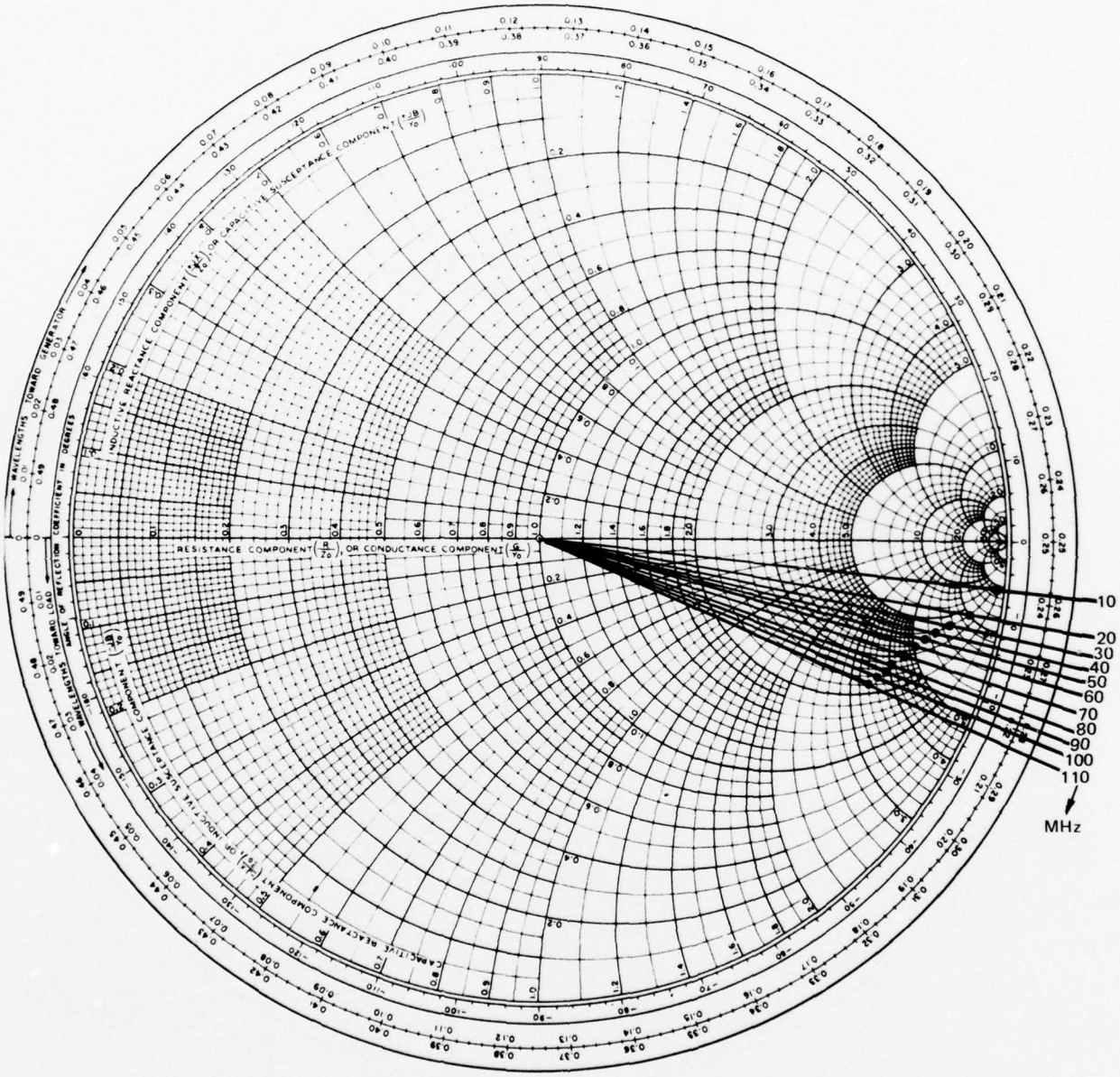

Figure 16. Ungrounded ZnO on silicon transducer.

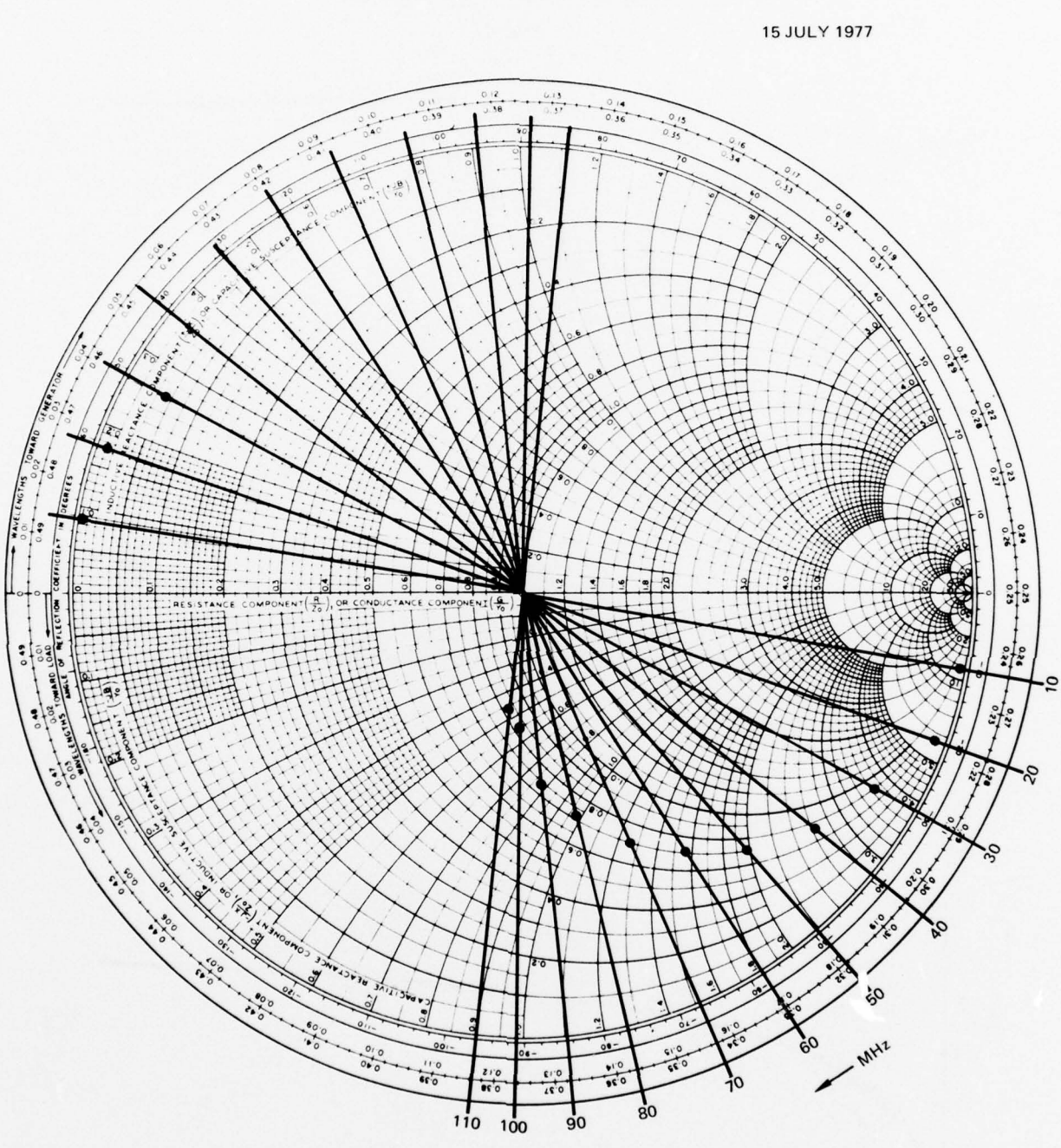

Figure 17. Grounded ZnO on silicon transducer.

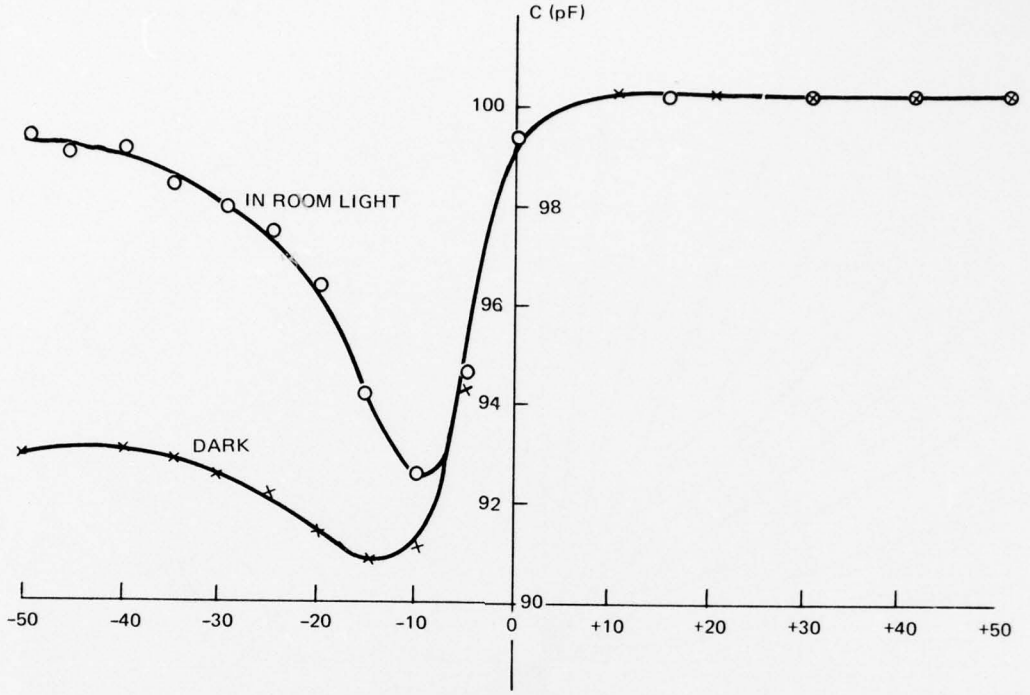

Figure 18. C-V characteristics of ZnO-on-silicon *transducer as a* function of light level.

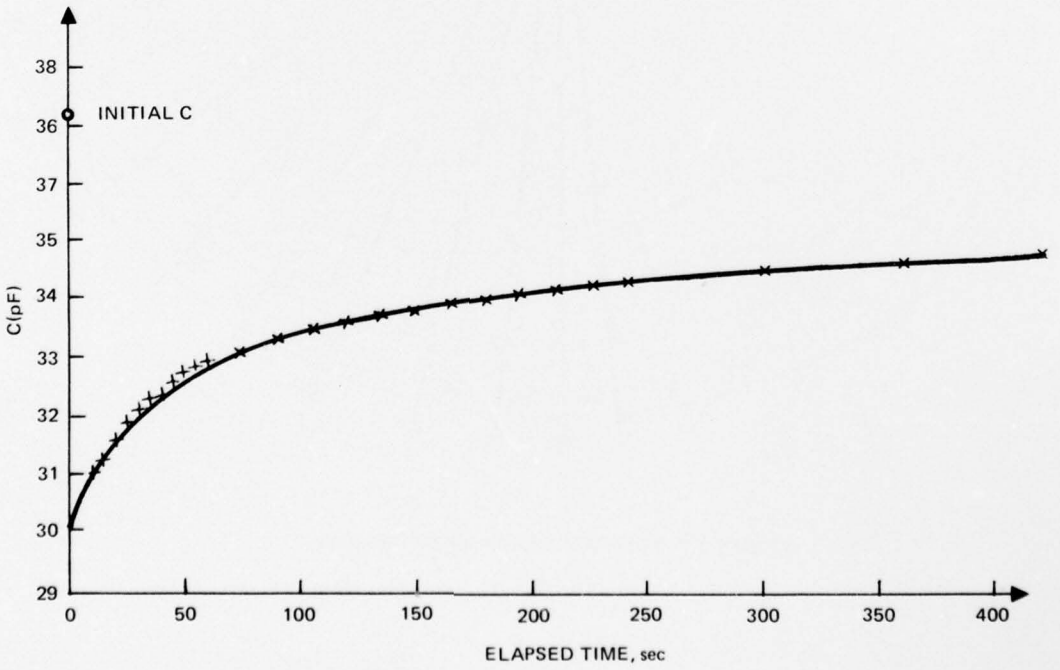

Figure 19. Charge of depletion capacitance of solid tap with time following inversion.

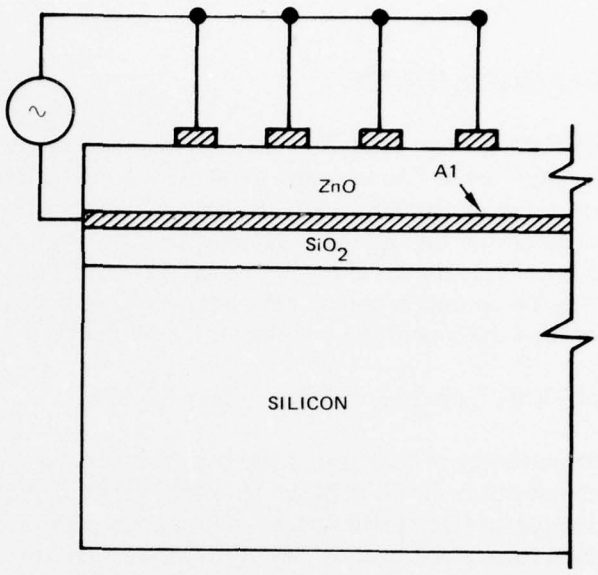

Figure 20. A useful transducer geometry for zinc oxide on silicon devices.

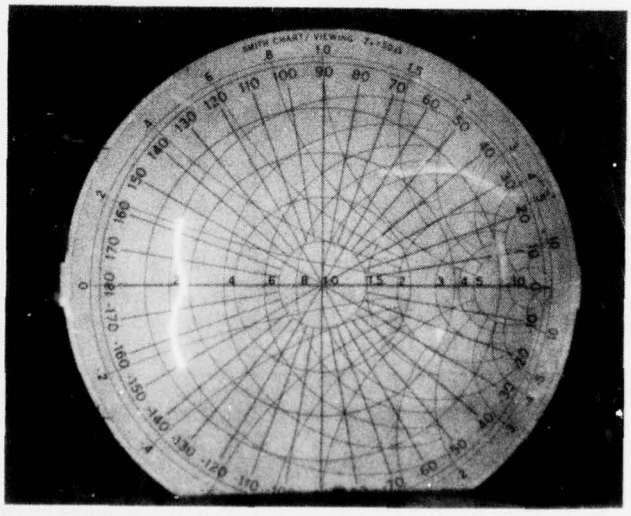

Figure 21. Impedance of an 80-megahertz ZnO-on-silicon transducer with interface electrode.

NONLINEAR INTERACTIONS

FOUR-TAP DEGENERATE DEVICE

Once efficient launching of SAWs onto silicon was achieved, some prototype triple-product convolvers were built. The first successful convolver was designed for 80-megahertz carrier frequencies at both delay line inputs to give a 160-megahertz product output at four MOS taps. One advantage of this approach (degenerate) over that of using two different carrier frequencies (nondegenerate) at the inputs and extracting the difference frequency product term is that the second harmonic term has no spatial variations. This can be stated mathematically as the vanishing of the k vector of the product:

$$\exp [j(\omega t - kx)] \cdot \exp [j(\omega t + kx)] = \exp (j2\omega t) \quad .$$

This eliminates the necessity of having spatially periodic MOS taps. A schematic of the four-tap degenerate device is shown in figure 22, while figure 23 pictures the experimental setup used to demonstrate electrically variable convolution with the device. During operation, an 80-megahertz signal generator is pulsed to feed one input transducer and is run CW into the other input transducer. The second harmonic signal at 160 megahertz is taken off the four center taps in parallel through an RF choke. The output signals for short and long input pulses are shown in figure 24; they represent convolution of the input pulse with

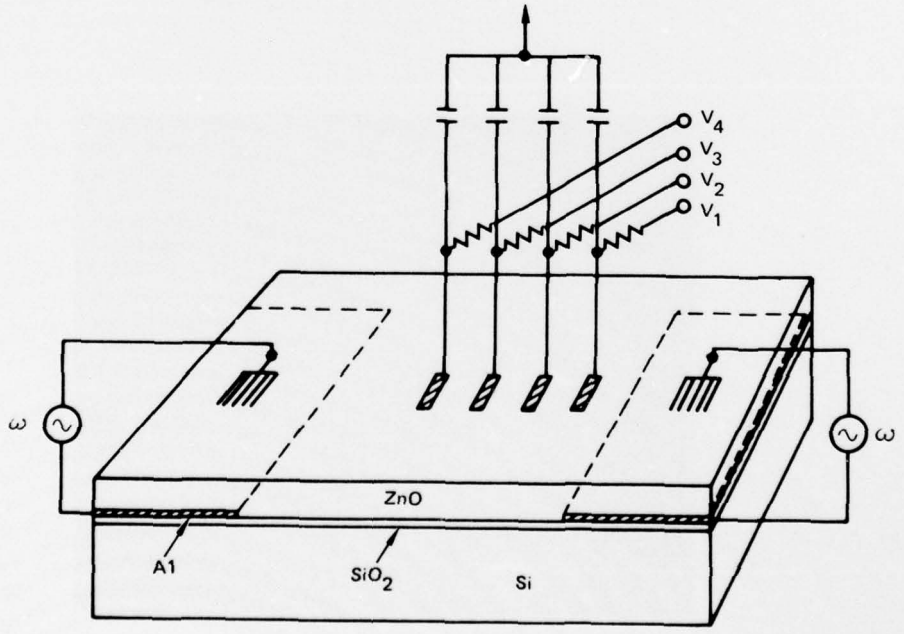

Figure 22. Four-tap triple-product convolver.

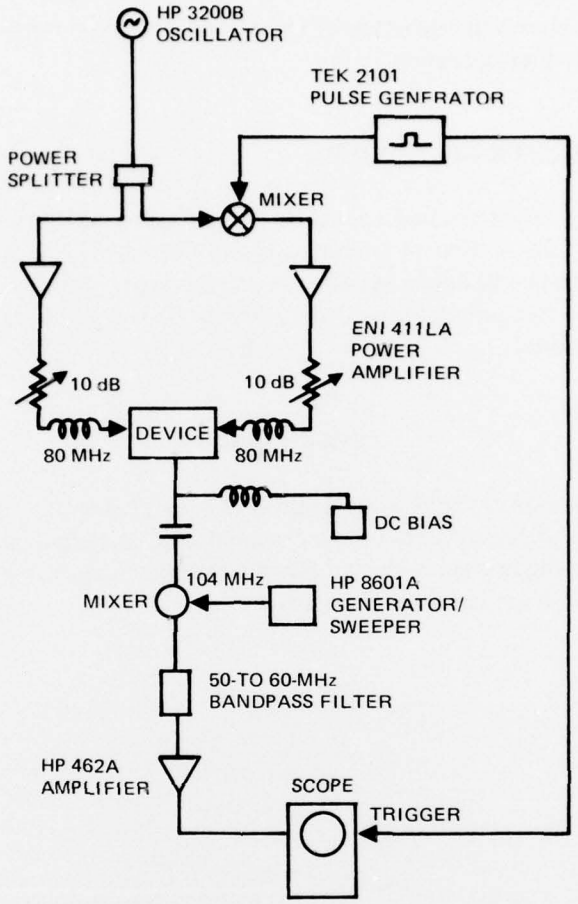

Figure 23. Experimental setup for observing triple-product convolution.

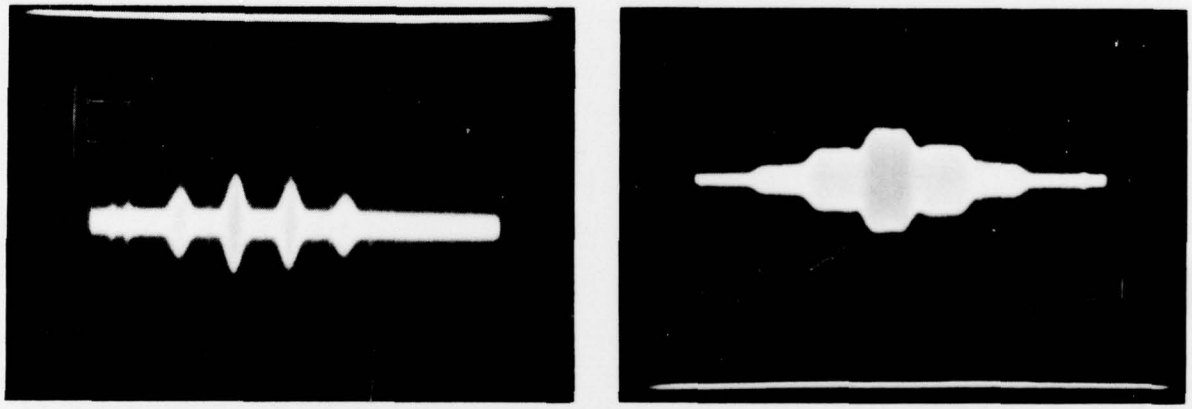

a. Scales: 20 millivolts per centimeter vertical
0.5 microsecond per centimeter horizontal.

b. Scales: 50 millivolts per centimeter vertical
0.5 microsecond per centimeter horizontal.

Figure 24. Convolution output of four-tap degenerate device for short and long pulses.

the taps. Figure 25 shows the variation of the second harmonic output with DC bias, illustrating triple-product operation.

SIXTEEN-TAP DEGENERATE DEVICE

A sixteen-tap triple-product convolver chip was also built, using 80-megahertz carrier frequencies. Convolution of a 1-microsecond pulse with eight uniformly biased taps of the convolver is shown in figure 26. The other eight taps, which are turned off, have no measurable effect on the convolution output. Figure 27 is a photograph of the sixteen-tap triple-product convolver.

CONCLUSIONS

Successful demonstrations of triple-product convolution have been made with four- and sixteen-tap ZnO silicon devices. Further work should include eliminating storage effects associated with trapping in the device and pursuing improvements in packaging and external circuitry to make these devices more practical.

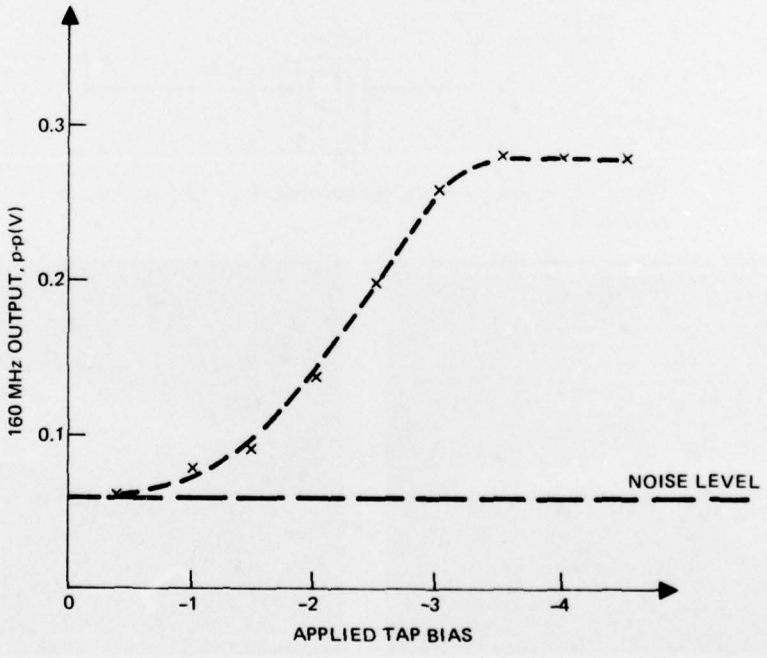

Figure 25. Variation of second harmonic output of four-tap degenerate convolver with DC bias.

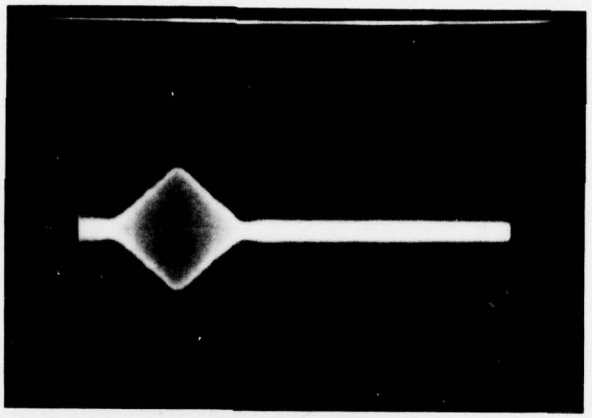

Figure 26. Convolution of a 1-microsecond pulse with eight uniformly biased taps of a sixteen-tap triple-product convolver.

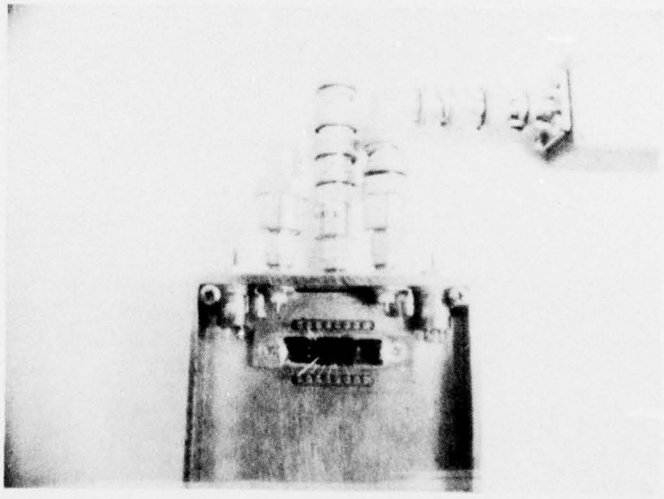

Figure 27. Photograph of sixteen-tap triple-product convolver.

REFERENCES

1. Reeder, T. M., "Fourier Transformation of Television Signals by Nonlinear Delay Line Techniques," United Aircraft Research Laboratories Technical Report N921957-F, March 1975.

2. Kino, G. S., and Gautier, H., "Convolution and parametric interaction with semiconductors," *J. Appl. Phys.*, vol. 44, no. 12, 5219 (1973).

3. Hickernell, F. S., and Brewer, J. W., "Surface-elastic-wave properties of dc-triode-sputtered zinc oxide films," *Appl. Phys. Lett.*, vol. 21, no. 8, 389 (1972).

4. Rozgonyi, G. A., and Polito, W. J., "Epitaxial thin films of ZnO on CdS and Sapphire," *J. Vac. Sci. Tech.*, vol. 6, no. 1, 115 (1969).

5. Khuri-Yakub, B. T., Kino, G. S., and Galle, P., "Studies of the optimum conditions for growth of rf-sputtered ZnO films," *J. Appl. Phys.*, vol. 46, no. 8, 3266 (1975).

6. Smith, H. I., Bachner, F. J., and Etremow, N., "A High-Yield Photolithographic Technique for Surface Wave Devices," *J. Electrochem. Soc.*, vol. 118, no. 5, 821 (1971).

7. Kino, G. S. and Wagers, R. S., "Theory of interdigital couplers on nonpiezoelectric substrates," *J. Appl. Phys.*, vol. 44, no. 4, 1480 (1973).

8. Fahmy, A. H., and Adler, E. L., "Multilayer acoustic-surface-wave program," *Proc. IEE*, vol. 122, no. 5, 470 (1975).

9. Coldren, L. A., "Effect of bias field in a zinc-oxide-on-silicon acoustic convolver," *Apl. Phys. Lett.*, vol. 25, no. 9, 473 (1974).

APPENDIX A. CIRCUIT MODEL OF PIEZORESISTIVE DEVICE

For a single tap, the high-frequency small-signal circuit for a piezoresistive MOSFET tap is as follows:

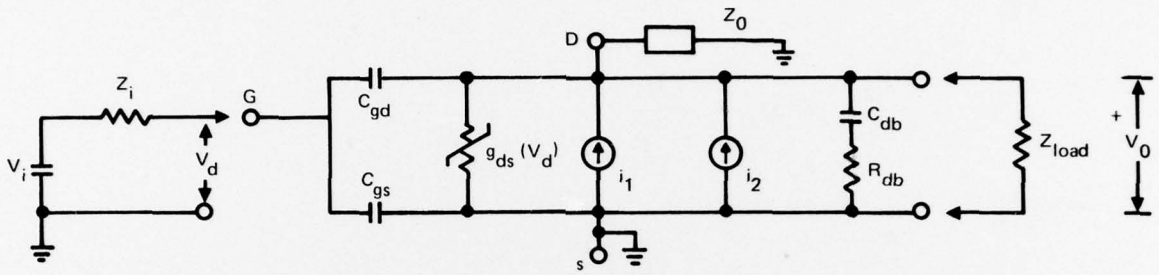

In this model $g_{ds}(V_d)$ is the nonlinear drain-source conductance associated with the MOSFET. The current generators i_1 and i_2 represent the linearly transduced surface acoustic waves, detected through the piezoresistance of the silicon inversion layer. The voltage source V_i represents the sampled input data voltage. The impedance Z_0 is the bias resistor in parallel with the remaining MOSFET tap impedances.

Since V_i is considered to be slowly varying with respect to the DFT components, the above circuit may be transformed thusly:

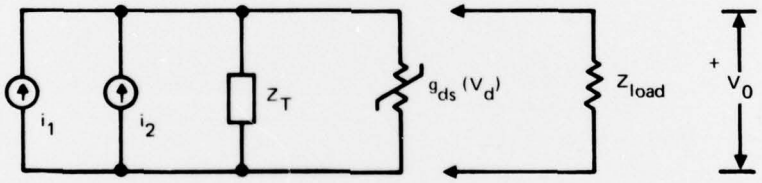

This circuit is identical to that analyzed by Reeder[1] for his diode array DFT. Following his approach

$$g_{ds}(V_d) \approx G_0 + G_1 V_d \ ,$$

where G_0 and G_1 are determined from the I_D vs. V_D curves for the MOSFET and represent the RF conductance and quadratic coupling coefficient, respectively.

From Reeder's analysis (for difference frequency operation)

$$V_0 \underset{\sim}{\propto} \frac{G_1}{G_0^3} \ Vg_1 \ Vg_2^* \ .$$

1. Reeder, T. M., "Fourier Transformation of Television Signals by Nonlinear Delay Line Techniques," United Aircraft Research Laboratories Technical Report N921957-F, March 1975.

where Vg_1 and Vg_2 are the equivalent voltage sources representing the amplitude of the transduced SAW at frequencies ω_1 and ω_2. Thus for a given data input voltage, the device output is proportional to the product of the two input chirp amplitudes. The dependence of $\frac{G_1}{G_0^3}$ on the input data voltages, however, appears to be highly nonlinear. First:

$$G_0 = \frac{\partial I_D}{\partial V_D} \quad \text{and} \quad G_1 = \frac{\partial I_D}{\partial V_D} \quad .$$

For a MOSFET just before saturation:

$$I_D = k \left[(V_G - V_T) V_D - \frac{V_D^2}{2} \right] \quad .$$

In this case

$$V_d = V_G$$
$$G_0 = k \left[(V_G - V_T) - V_D \right]$$
$$G_1 = -k \quad .$$

Consequently

$$V_0 \underset{\sim}{\propto} \frac{Vg_1 \, Vg_2^*}{\left[(V_G - V_T) - V_D \right]^3}$$

and V_0 has a highly nonlinear relationship to $V_G = V_d$.

APPENDIX B.
CALCULATION OF POTENTIALS IN ZINC-OXIDE SUBSTRATE

In regions (1) and (2), no free charge is assumed:

$$\nabla^2 \Phi = 0$$

$$\Phi_1 (y) = C_1 + C_2$$

$$\Phi_2 (y) = C_3 y + C_4$$

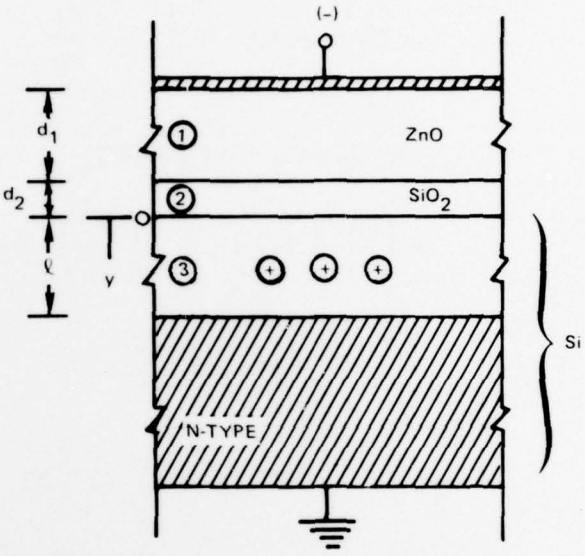

In region (3), an ionized donor charge

$$\nabla^2 \Phi_3 = - \rho/\epsilon_3 = - \frac{q N}{\epsilon_3}$$

$$\Phi_3 (y) = - \frac{q N}{2 \epsilon_3} y^2 + C_5 y + C_6$$

B.C.'s

1. $$- \epsilon_1 \left.\frac{d\Phi_1}{dy}\right|_{y=-(d_1+d_2)} = -qN\ell$$

2. $$\epsilon_1 \left.\frac{d\Phi_1}{dy}\right|_{y=-d_2} = \epsilon_2 \left.\frac{d\Phi_2}{dy}\right|_{y=-d_2}$$

3. $$\Phi_1 (-d_2) = \Phi_2 (-d_2)$$

4. $$\epsilon_2 \left.\frac{d\Phi_2}{dy}\right|_{y=0} = \epsilon_3 \left.\frac{d\Phi_3}{dy}\right|_{y=0}$$

5. $$\Phi_2 (0) = \Phi_3 (0)$$

6. $$\Phi_3 (\ell) = 0$$

$$-\epsilon_1 C_1 = -qN\ell \Rightarrow \boxed{C_1 = \frac{qN\ell}{\epsilon_1}}$$

$$\epsilon_1 C_1 = \epsilon_2 C_3 \Rightarrow \boxed{C_3 = \frac{\epsilon_1}{\epsilon_2} \cdot \frac{qN\ell}{\epsilon_3} = \frac{qN\ell}{\epsilon_2}}$$

$$-C_1 d_2 + C_2 = -C_3 d_2 + C_4$$

$$-\left(\frac{qN\ell}{\epsilon_1}\right) d_2 + C_2 = -\left(\frac{qN\ell}{\epsilon_2}\right) d_2 + C_4$$

$$C_2 - C_4 = \frac{qN\ell}{C_1} d_2 - \frac{qN\ell}{\epsilon_2} d_2 = qN\ell \left(\frac{d_2}{\epsilon_1} - \frac{d_2}{\epsilon_2}\right)$$

$$C_2 - C_4 = qN\ell\, d_2 \left(\frac{1}{\epsilon_1} - \frac{1}{\epsilon_2}\right)$$

$$\epsilon_2 C_3 = \epsilon_3 C_5 \Rightarrow \boxed{C_5 = \frac{\epsilon_2}{\epsilon_3} - \frac{qN\ell}{\epsilon_2} = \frac{qN\ell}{\epsilon_3}}$$

$$\boxed{C_4 = C_6}$$

$$-\frac{qN}{2\epsilon_3} \ell^2 + C_5 \ell + C_6 = 0$$

$$\Rightarrow \boxed{C_6} = \frac{qN}{2\epsilon_3} \ell^2 - C_5 \ell = \frac{qN}{2\epsilon_3} \ell^2 - \frac{qN\ell^2}{\epsilon_3} = \boxed{-\frac{qN\ell^2}{2\epsilon_3}}$$

$$= C_4$$

$$C_2 = C_4 + qN\ell\, d_2 \left(\frac{1}{\epsilon_1} - \frac{1}{\epsilon_2}\right)$$

$$\boxed{C_2 = -\frac{qN\ell^2}{2\epsilon_3} + qN\ell\, d_2 \left(\frac{1}{\epsilon_1} - \frac{1}{\epsilon_2}\right)}$$

thus

$$\boxed{\Phi_1(y) = \frac{qN\ell}{\epsilon_1}\, y - \frac{qN\ell^2}{2\epsilon_3} + qN\ell\, d_2 \left(\frac{1}{\epsilon_1} - \frac{1}{\epsilon_2}\right)}$$

$$\boxed{\Phi_2(y) = \frac{qN\ell}{\epsilon_2}\, y - \frac{qN\ell^2}{2\epsilon_3}}$$

$$\boxed{\Phi_3(y) = -\frac{qN}{2\epsilon_3}\, y^2 + \frac{qN\ell}{\epsilon_3}\, y - \frac{qN\ell^2}{2\epsilon_3}}$$

Variation of gate voltage with surface potential

$$\Phi_1(-d_1 - d_2) = V_G = -\frac{qN\ell}{\epsilon_1}(d_1 + d_2) - \frac{qN\ell^2}{2\epsilon_3} + qN\ell\, d_2 \left(\frac{1}{\epsilon_1} - \frac{1}{\epsilon_2}\right)$$

$$V_G = -\frac{qN\ell^2}{2\epsilon_3} - \ell \left[\frac{qN}{\epsilon_1}(d_1 + d_2) - qN\, d_2 \left(\frac{1}{\epsilon_1} - \frac{1}{\epsilon_2}\right)\right]$$

or

$$V_G = -\frac{qN\ell^2}{2\epsilon_3} - \ell \left\{\frac{qN\, d_1}{\epsilon_1} + \frac{qN\, d_2}{\epsilon_2}\right\}$$

$$\boxed{V_G = -\frac{qN\ell^2}{2\epsilon_3} - qN\ell \left(\frac{d_1}{\epsilon_1} + \frac{d_2}{\epsilon_2}\right)}$$

APPENDIX C. LIFT-OFF PHOTOLITHOGRAPHIC PROCEDURE

1. Clean substrate by swabbing with lab soap (Liquinox), rinsing in deionized water, and boiling in deionized water.

2. Bake-out slides for 1 hour.

3. Let substrate cool to room temperature.

4. Flood substrate with filtered AZ 1350 B photoresist.

5. Spin at 3000 rpm for 30 seconds.

6. Bake-out at 90°C for 25 minutes.

7. Cool for 10 minutes to room temperature.

8. Expose through mask using vacuum pulldown for 220 seconds (11-inch mask-to-light separation).

9. Develop for 35 seconds in MF-312 developer, 1:1 with deionized water at room temperature.

10. Rinse for 1 minute in deionized water.

11. Deposit 300 angstroms of Ti and about 1000 angstroms of other metal on photoresist pattern. Ultimate vacuum should be around 5×10^{-8} torr.

12. Lift-off with 50°C acetone accompanied by light swabbing with a cotton swab. Acetone may be decanted to eliminate large pieces of metal initially lifted off.

13. Rinse in deionized water.

APPENDIX *D.*
EFFECT OF PACKAGE CAPACITANCE ON TRANSDUCER IMPEDANCE

(from discussion with Dr. Eric Adler)

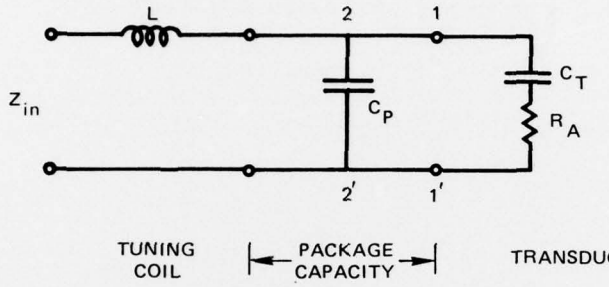

Assumptions: Radiation $Q_R = \dfrac{1}{\omega R_A C_T} >> 1$ [otherwise need shunt model]

$$Z_{22}' = \frac{1}{j\omega C_P + \dfrac{1}{R_A + \dfrac{1}{j\omega C_T}}}$$

$$= \frac{1}{j\omega C_P + \dfrac{R_A - 1/j\omega C_T}{R_A^2 + \left(\dfrac{1}{\omega C_T}\right)^2}}$$

neglect from high Q_R assumption

$$\simeq \frac{1}{j\omega C_P + R_A(\omega C_T)^2 + j\omega C_T}$$

$$= \frac{R_A(\omega C_T)^2 - j\omega(C_P + C_T)}{[R_A(\omega C_T)^2]^2 + [\omega(C_P + C_T)]^2}$$

neglect for same reason as above

$$Z_{22}' = R_A \left(\frac{C_T}{C_P + C_T} \right)^2 - \frac{j}{\omega [(C_P + C_T)]}$$

If coil tunes out $C_P + C_T$ then

$$\text{Re } Z_{in} = R_A \left(\frac{C_T}{C_P + C_T} \right)^2$$ and a reduction always occurs.

APPENDIX E.

ESTIMATE OF INSERTION LOSSES FOR SILICON DEVICES (WITH AND WITHOUT A BULK LOSS TERM).

An approximate model of a standard transducer-plus-connector capacitance at resonance is as follows:

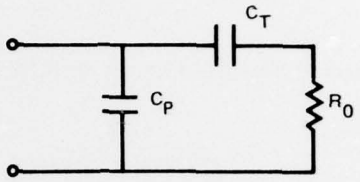

This reduces approximately to the following according to Adler's approximation:

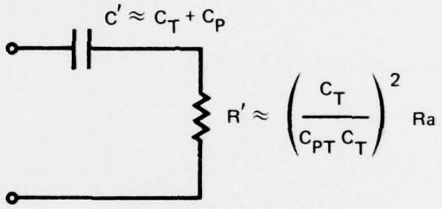

The circuit of interest is then:

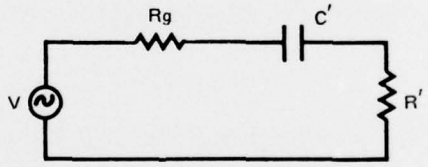

The maximum power available to the load is

$$\frac{V^2}{4\,Rg}$$

and the power absorbed in the load is

$$\frac{V^2\,R'}{(R' + Rg)^2 + \left(\frac{1}{\omega\,C'}\right)^2}$$

Therefore the power mismatch is given by:

$$P_M = \frac{4\,R'\,Rg}{(R' + Rg)^2 + \left(\frac{1}{\omega\,C'}\right)^2}$$

For an estimate of the insertion loss, assume that $R_a = 50\,\Omega$, $C_T = 1$ pF, $C_P = 10$ pF, and $Rg = 50\,\Omega$.

An estimate of the untuned mismatch loss is then (for $\omega = 100$ MHz):

$$\frac{4\,(0.5)\,(50)}{(0.5 + 50)^2 + (150)^2} \approx \frac{100}{2500 + 22500} = \frac{100}{25000} = \frac{1}{250}$$

This corresponds to approximately 24 dB mismatch loss. The two way insertion loss is approximately:

$$2\,(24) + 6 \text{ (bidirectionality loss)} = 54 \text{ dB untuned.}$$

An estimate of the tuned mismatch loss is:

$$\frac{4\,(0.5)\,(50)}{(0.5 + 50)^2} = \frac{100}{2500} = \frac{1}{25}$$

This corresponds to approximately 14 dB mismatch loss. The two way insertion loss is approximately:

$$2\,(14) + 6 = 34 \text{ dB tuned.}$$

Now assume that R_a consists of an acoustic part, R_A, and a bulk loss part, R_B. Say $R_B \approx 100\,R_A$

and

$$R_A = 50\,\Omega,\ R_B = 5000\,\Omega,\ R_A' = 0.5\,\Omega,\ R_B' = 50\,\Omega.$$

An estimate of the tuned mismatch loss is then:

$$\frac{4\,(0.5)\,(50)}{(50 + 50)^2} = \frac{100}{10000} = \frac{1}{100} = 20 \text{ dB mismatch loss.}$$

This gives $2\,(20) + 6 = 46$ dB tuned insertion loss.

Thus the presence of a bulk loss term does not significantly affect the untuned insertion loss, but a large discrepancy is observed in the tuned insertion loss if the bulk resistance is not taken into account.